


Polymer Membranes for Enthalpy Exchangers

Kamil Križo, Andrej Kapjor and Michal Holubčík * 

Department of Power Engineering, Faculty of Mechanical Engineering, University of Zilina, Univerzitná 8215, 010 26 Žilina, Slovakia

* Correspondence: michal.holubcik@fstroj.uniza.sk

Abstract: A membrane-based enthalpy exchanger is a device used for heat and humidity recovery in ventilated buildings. The energy-saving potential of such a device is dependent on the parameters responsible for heat and moisture recovery. The trend is toward composite membranes, which are custom produced, and their parameters can be adjusted for a given application; therefore, the diffusion and sorption characteristics of such membranes are unknown. In order to obtain the values of the water vapor diffusivity of three investigated handmade membranes, a serial resistance model using a Field and Laboratory Emission Cell (FLEC) is proposed. Experiments were conducted to identify the resistance in each step of the moisture transfer process to extract the moisture diffusivity in the membranes. The calculated moisture diffusivities in the membranes were 8.99×10^{-12} (m²/s) for the membranes from cellulose acetate, 1.9×10^{-10} (m²/s) for the microporous PE/PUR membranes, and 1.53×10^{-11} (m²/s) for the PET/PUR microfibrinous membranes. The obtained membrane diffusivities were then used in the proposed effectiveness-NTU-based model of an exchanger with a cross-flow arrangement to predict performance under various operating conditions. The results show that the highest latent effectiveness was found for the exchanger core made from the PE/PUR membrane and the lowest was for the one with the PE/PUR membrane core.

Keywords: enthalpy exchanger; mass transfer; polymer membranes; water vapor diffusivity



Citation: Križo, K.; Kapjor, A.; Holubčík, M. Polymer Membranes for Enthalpy Exchangers. *Energies* **2022**, *15*, 6021. <https://doi.org/10.3390/en15166021>

Academic Editors: Anatoliy Pavlenko and Hanna Koshlak

Received: 14 July 2022

Accepted: 17 August 2022

Published: 19 August 2022

Publisher's Note: MDPI stays neutral with regard to jurisdictional claims in published maps and institutional affiliations.



Copyright: © 2022 by the authors. Licensee MDPI, Basel, Switzerland. This article is an open access article distributed under the terms and conditions of the Creative Commons Attribution (CC BY) license (<https://creativecommons.org/licenses/by/4.0/>).

1. Introduction

The increase in energy market prices and the increased impact of human development on global warming have forced governments around the world to increase the requirements for energy-related products. For energy recovery systems, it means developing more efficient and environmentally friendly products. A large portion of energy consumption is building ventilation. A portion of this energy demand is from air conditioning, such as heating in winter and cooling in summer. Recently, there have been discussions about the implementation of moisture recovery in energy-related product ratings due to latent heat representing a large portion of the total thermal load of an air-conditioned building [1].

To recover both the sensible and latent heat from the exhaust air in buildings, two main air-to-air exchanger types are used. A rotary exchanger, although it has the highest total effectiveness, cannot provide a 100% clean supply air. The reason for this is its design, which causes leakage between the supply and exhaust air. These hygienic requirements have received increased attention during the ongoing COVID-19 pandemic. To minimize the risk, a membrane-based plate exchanger can be used where there is no risk of mixing between the airstreams. Unlike sensible plate exchangers, the plates of an enthalpy exchanger are made from semipermeable polymer membranes instead of metal or plastic. This type of exchanger recovers sensible and latent heat simultaneously. In Europe, where the latent load is lower than in southwest Asia, an enthalpy exchanger can be utilized to recover moisture from the exhaust air and moisturize the dry supply air in the winter months. On top of this, when operating under conditions with below-freezing temperatures, the icing of an exchanger is less likely due to the rapid dehumidification of the extract air, which hardly reaches the dew point.

For energy recovery purposes, it is most important to investigate the moisture transport properties of membranes. As mentioned by Dugaria et al. [2], the heat conductivity of the plate material does not play a significant role in sensible heat recovery. Under considered conditions, the ratio of the conductive to convective resistance in the plate boundary layer is less than 1/100. There is also a minor influence of the plate thickness on sensible effectiveness if it is kept relatively thin (up to 120 μm). Therefore, more investigations are devoted to the moisture transport in the membranes.

For a long time, the most common material for enthalpy exchanger fabrication has been paper. Zhang et al. [3] reported the value of the water vapor diffusivity in paper to be $6.08 \times 10^{-12} \text{ m}^2/\text{s}$, which is much lower than that in polymeric membranes. Lee et al. [4] enhanced the diffusivity of paper by impregnating it with lithium chloride (LiCl). The reported values of the moisture diffusivity ranged from $1.8 \times 10^{-11} \text{ m}^2/\text{s}$ to $6.0 \times 10^{-11} \text{ m}^2/\text{s}$ and in another study, it was found to be $3.8 \times 10^{-11} \text{ m}^2/\text{s}$ [5].

Much attention has been paid to cellulose acetate (CA) as a cheap and available material, with evaluated diffusivity values of $1.05 \times 10^{-11} \text{ m}^2/\text{s}$ [3]. In another report, Zhang et al. mentioned that the diffusivity of machine-made CA was $3.77 \times 10^{-6} \text{ kg}/\text{m}\cdot\text{s}$ and that of handmade CA was $4.76 \times 10^{-6} \text{ kg}/\text{m}\cdot\text{s}$ [6].

Other cellulose derivatives have been investigated by Zhang, where the diffusivity of modified cellulose was $2.50 \times 10^{-10} \text{ kg}/\text{m}\cdot\text{s}$ [3] and that of mixed cellulose was $3.60 \times 10^{-10} \text{ m}^2/\text{s}$ [7]. The reported diffusivity of cellulose by Min was $7.83 \times 10^{-7} \text{ kg}/\text{m}\cdot\text{s}$ [8].

Other homogenous polymer films have been investigated by Niu and Zhang with the diffusivity in a copolymer membrane found to be $2.16 \times 10^{-8} \text{ kg}/\text{m}\cdot\text{s}$. For polyether-sulfone (PES), it was $7.10 \times 10^{-7} \text{ kg}/\text{m}\cdot\text{s}$ and for polyvinylidene fluoride (PVDF) it was $1.92 \times 10^{-6} \text{ kg}/\text{m}\cdot\text{s}$ [8].

Recently, more attention has been focused on composite membranes, mainly due to the independent preparation and optimization of the selective layer and porous substrate. The diffusivity of a composite membrane reported by Huizing was $3.3 \times 10^{-11} \text{ m}^2/\text{s}$ for a hydrophilic polymer film and $1.13 \times 10^{-10} \text{ m}^2/\text{s}$ for a microporous substrate [9]. The two-layered structure of a polyvinylidene fluoride and polyvinyl alcohol (PVDF/PVAL) membrane was investigated by Zhang and the diffusivity was found to be $3.2 \times 10^{-11} \text{ m}^2/\text{s}$ [10].

Standard moisture diffusivity measurements are performed using gravimetric methods that record the weight loss of the sample exposed to a range of air humidities. The effective diffusivity is obtained by direct permeation tests under steady-state conditions. Both methods, although widely used, often neglect the convective resistance in the boundary layer, which leads to inaccurate results. The shortcomings of the aforementioned methods encouraged authors Zhang [7,11] and Min et al. [8] to develop a new approach to evaluating moisture diffusivity in the membranes by considering the effect of the boundary layer on both sides of the membrane.

2. Setup

In this study, a step-by-step approach based on the methods described by Zhang and Min et al. is used to evaluate the individual resistance of humidity transfer in three handmade polymeric membranes. A simple mathematical model is described to calculate the moisture diffusivity in the membrane using experimentally sampled data. As a moisture exchanger, a Field and Laboratory Emission Cell (FLEC) was used. A FLEC is designed for the volatile organic compounds (VOC) emission testing of material surfaces. Its shape promotes efficient airflow over the tested specimen. The FLEC's inner chamber is in the form of a cone-shaped cavity promoting an even velocity profile along the cell radius and thus an even emission rate across the tested surface. The low slit height forces the air to flow close to the membrane surface to be efficiently humidified [7,11].

Test Rig

The scheme of the test rig is presented in Figure 1. Clean, dehumidified air is supplied from a compressed air bottle. The volume flow is controlled by flow meters and adjusted

by a needle valve. Due to compressed air being almost completely dry, a portion of the supply air is separated and humidified by a bubbler before being mixed with dry air. This process allows for the preparation of supply air with the desirable 5% relative humidity. The temperature is kept constant by placing the test rig in an air-conditioned room. The temperature, humidity, and volume flow of the air are measured by sensors placed in the chambers of the inlet and outlet of the cell. The bottom chamber of the cell is filled with distilled water, providing a humidity source for the supply air to be moisturized. Pressure meters are used to control the pressure in the rig.

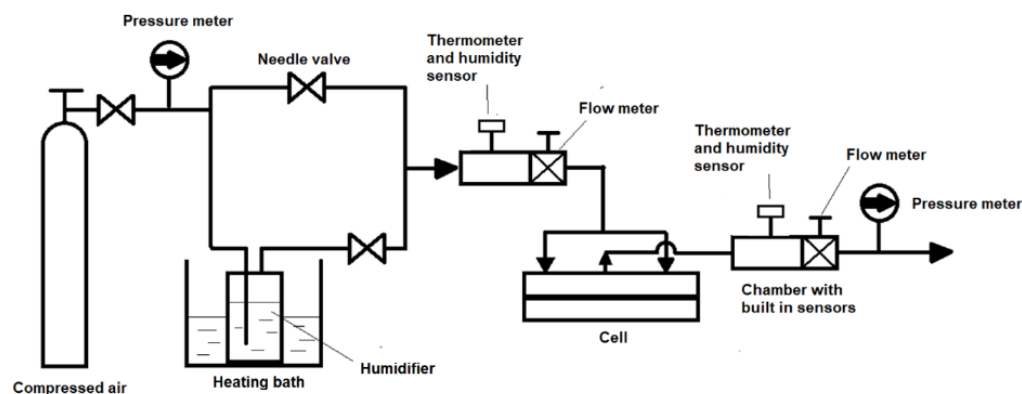


Figure 1. Scheme of the test rig.

Measurements were conducted under a constant temperature of 22 °C, within a ± 1 °C temperature range. During the experiments, the volume flow yielded 2–6 L/min. The inlet's relative humidity was kept constant at 5% for all the experiments to create higher gradients of humidity in the inlet and outlet of the cell. The measured pressure drop of the rig ranged from 9.6 to 47 kPa. The calculated mean velocity ranged from 0.07 to 0.22 m/s. The humidity was measured by a temperature/humidity sensor Pt100, class A, with a sensor precision of ± 0.2 Kelvin at 23 °C and $\pm 1.3\%$ RH at 23 °C. The volume flow was measured by a ball flow meter with a precision of $\pm 5\%$. The pressure was measured by membrane pressure meters with a precision of $\pm 0.5\%$ FS. Technical specification of the FLEC is summarized in Table 1.

Table 1. Technical specifications of the FLEC [12].

Volume (m ³)	3.5×10^{-5}			
Maximum emission area (m ²)	0.0177			
Inner minimum height (mm)	1			
Cell diameter (mm)	150			
Inner maximum height (mm)	18			
Volume flow (L/min)	0.1	0.3	1.4	2.8
Exchange rate h ⁻¹	171	514	2400	4800

3. Materials and Properties

Three membrane samples were prepared to undergo water vapor diffusivity testing. The membrane samples were produced from cheap, easy-to-obtain materials, with no harsh chemicals used in their fabrication.

The asymmetric cellulose acetate membrane was prepared using the one-step fabrication process from the wet phase inversion method described by Zhang et al. [13].

In Figure 2, the changing structure in the membrane cross-section transferred from the macroporous finger-like structure to the dense, porous structure can be seen. The membrane structure can be adjusted in the fabrication process using different ratios of additive (deionized water) to casting solution [13]. The created membrane was a self-supporting asymmetric membrane with expected good selectivity to unwanted gasses. The thickness of the fabricated membrane was 20 μm .

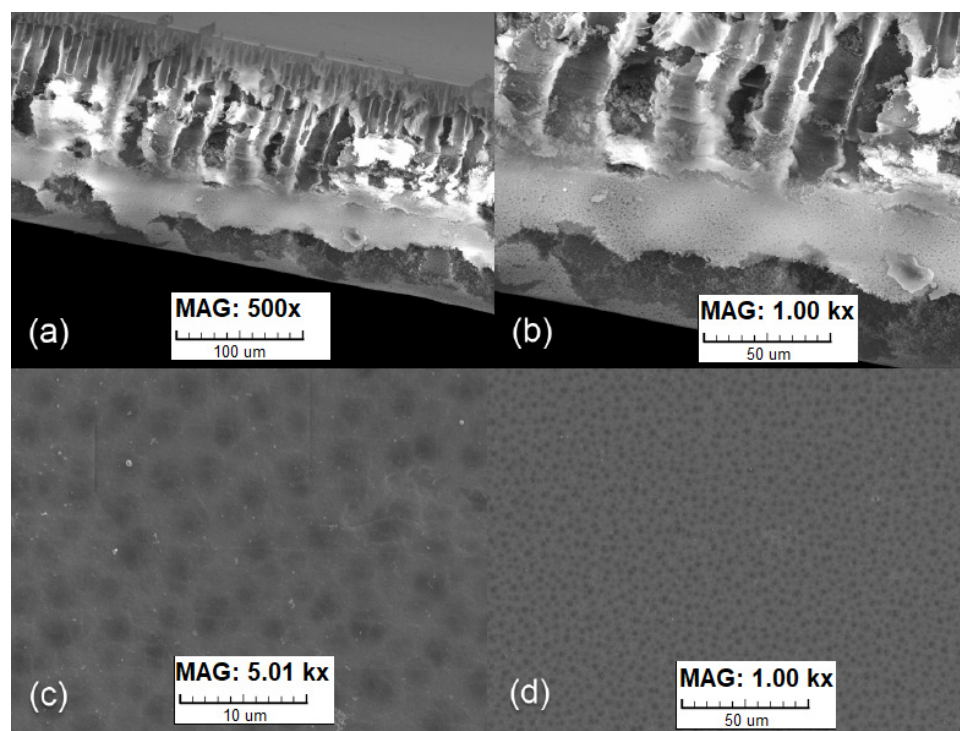


Figure 2. SEM images of cellulose acetate (CA) (a,b) membrane cross-section, (c,d) membrane surface under 500 \times , 1000 \times , and 5000 \times magnifications.

The other two membrane samples were fabricated by coating a hydrophilic polymer onto a hydrophobic substrate to create a two-layer composite membrane.

The polyethylene/polyurethane (PE/PUR) membrane was prepared by coating a waterborne polyether polyurethane dispersion onto a silica-filled nanoporous polyethylene substrate. The substrate was a dimensionally stable, highly porous synthetic material with good absorption of coatings and adhesives. The use of a polyurethane coating containing a soft polyethylene oxide (PEO) block on microporous and nanofibrous substrates was described by Huizing [14,15]. The advantage of coated composite membranes is the possibility of the independent selection of materials for the selective and support layers, which causes a higher moisture flux. To create the very thin layer, a 15% polymer/water solution was prepared and coated onto the substrate using a casting knife. The coated membrane was dried at room temperature. Afterward, the membrane was cured at 100 °C for 4 h. The thickness of the fabricated membrane after coating was 150 μm . The morphology of the fabricated membrane was observed using scanning electron microscopy (SEM). In Figure 3, a cross-section of the membrane with a microporous structure, as well as continuous dense coating without deflections, can be seen.

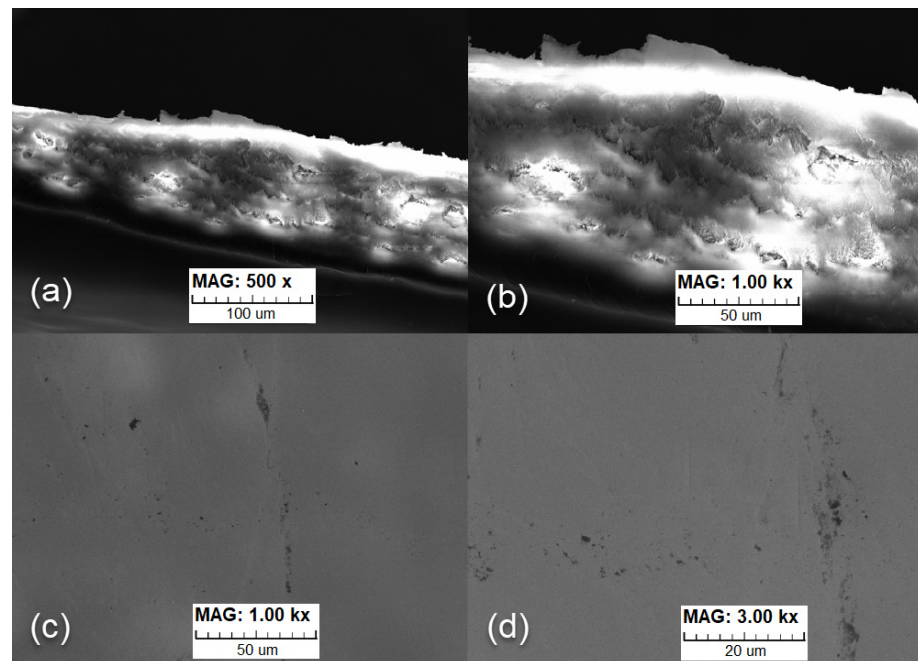


Figure 3. Images of composite PE/PUR membrane (a,b) cross-section and (c,d) surface under 500 \times , 1000 \times , and 3000 \times magnifications.

Figure 4 shows the polyester/polyurethane (PET/PUR) membrane produced by coating the same dispersion onto a thin polyester fibrous nonwoven fabric. In this case, a 5% water solution was prepared and coated onto the membrane using a rubber wiper. The membrane was dried at room temperature and cured at 100 °C for 4 h. The thickness of the coated membrane was 20 μm .

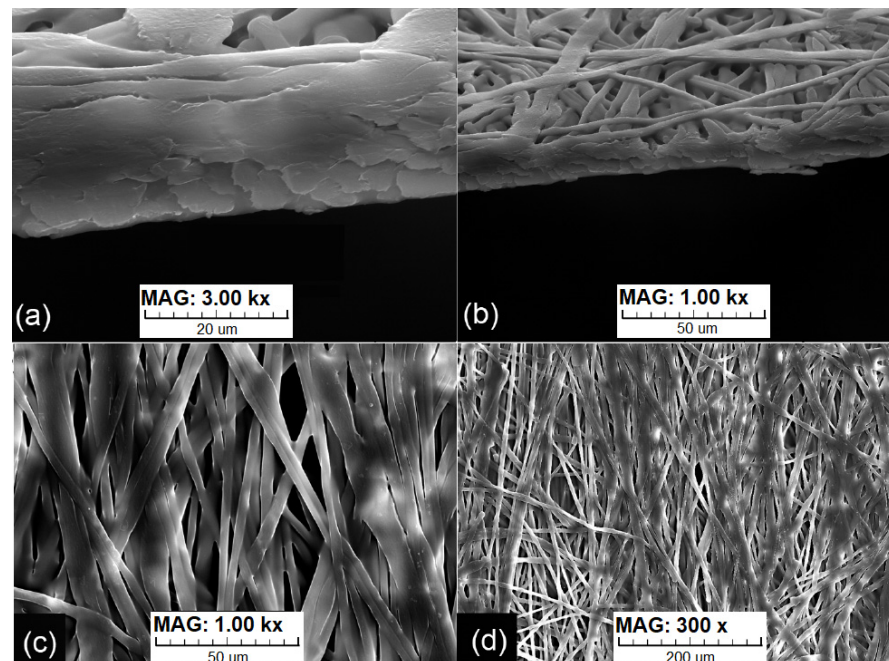


Figure 4. SEM images of composite PET/PUR membrane (a,b) cross-section (c,d) surface under 300 \times , 1000 \times , and 3000 \times magnifications.

The sorption properties of the membranes summarized in Table 2 were obtained using gravimetric measurements at 20 °C by a water vapor sorption analyzer DVS Adventure.

Other material properties, such as density and heat conductivity, were obtained from the material datasheets provided by the manufacturer.

Table 2. Values of membrane properties.

Membrane	δ_m (μm)	λ_m (W/m·K)	ρ	ω_{max} (kg/kg)	C
Polyethylene/Polyurethane PE/PUR	150	0.33	630	0.09	2.4
Cellulose Acetate CA	20	0.17	870	0.42	0.76
Polyethylene terephthalate/Polyurethane PET/PUR	20	0.05	722.6	0.12	0.88

4. Data Reduction

The moisture transfer in the membrane is governed by a well-known solution–diffusion mechanism [16]. The correlations in this section were adopted from Min [8] and Zhang [17].

Vaporized water from the saturated air layer above the water surface diffuses through the air gap below the membrane and is absorbed by the membrane’s bottom surface. The water vapor permeation rate J (kg/m·s) is expressed as

$$J = \frac{D_{va}}{L}(\omega_s - \omega_{mw}) \quad (1)$$

where D_{va} is the equivalent vapor diffusivity in the air gap (m^2/s) and L is the gap height (m). The moisture absorbed into the membrane is diffused through the membrane thickness on the side of the flowing air. The permeation rate of the water vapor across the membrane is expressed as

$$J = \frac{D_{wm}}{\delta_m}(\theta_{mw} - \theta_{ma}) = \frac{D_{wm}}{\delta_m} \frac{\theta_{mw} - \theta_{ma}}{\omega_{mw} - \omega_{ma}}(\omega_{mw} - \omega_{ma}) \quad (2)$$

where δ_m is the membrane thickness (m), D_{wm} is the water vapor diffusivity in the membrane ($\text{kg}/\text{m}^2\cdot\text{s}$), θ is the water uptake of the membrane (kg/kg), and ω is the humidity ratio in the air (kg/kg).

The diffused moisture collected on the membrane surface facing the flowing air is taken by convection, creating a humidity gradient between the inlet and outlet air. The permeation rate between the membrane surface and the flowing air is expressed as

$$J = k(\omega_{ma} - \omega_a) \quad (3)$$

where k is convective mass transfer coefficient (m/s), and ω_a is the average humidity ratio between the inlet and outlet air (kg/kg).

$$\omega_a = \frac{\omega_i + \omega_o}{2} \quad (4)$$

The above-described resistances can be summarized as the total mass transfer resistance:

$$R_T = \frac{1}{k} + \frac{D_{wm}}{\delta} \frac{\omega_{mw} - \omega_{ma}}{\theta_{mw} - \theta_{ma}} + \frac{L}{D_{va}} = R_c + R_m + R_g \quad (5)$$

The relationship between the permeation rate and total mass transfer resistance R_T ($\text{m}^2\cdot\text{s}/\text{kg}$) is

$$J = \frac{\omega_s - \omega_a}{R_T} \quad (6)$$

The total mass transfer resistance can be calculated from the measured humidity ratio difference between the inlet and outlet air and the logarithmic humidity ratio difference between the water surface and air stream.

$$R_T = \frac{A \Delta\omega}{(\omega_o - \omega_i)m_a} \quad (7)$$

The logarithmic humidity ratio difference between the saturated air above the water and the airstream is given by

$$\Delta\omega = \frac{(\omega_s - \omega_{in}) - (\omega_s - \omega_o)}{\ln\left(\frac{\omega_s - \omega_i}{\omega_s - \omega_o}\right)} \quad (8)$$

Finally, the water vapor diffusivity in the membrane ($\text{kg}/\text{m}^2 \cdot \text{s}$) can be obtained from the following equation:

$$D_{wm} = \frac{\delta}{R_m} \frac{(\omega_{mw} - \omega_{ma})}{(\theta_{mw} - \theta_{ma})} \quad (9)$$

where the humidity ratio at the membrane air side ω_{ma} can be expressed by Equations (3) and (6) after the convective mass transfer is obtained. The humidity ratio at the membrane's water side ω_{mw} can be expressed by Equations (1) and (6).

If the membrane density is known, the diffusivity can be expressed in units (m^2/s) by the following equation [17]:

$$D_{wm} = \frac{\rho_a \delta \psi}{\rho_m R_m} \quad (10)$$

where ψ is the dimensionless coefficient of the diffusive resistance for the membrane material presented by Zhang et al. [3].

$$\psi = \frac{10^6 (1 - C + C/RH)^2 RH^2}{e^{(5294/T)} \omega_{max} C} \quad (11)$$

The correlation between the equilibrium water uptake of the membrane and the relative humidity is given by:

$$\theta = \frac{\omega_{max}}{1 - C + \frac{C}{RH}} \quad (12)$$

where ω_{max} (kg/kg) represents the maximum moisture content of the water vapor in the membrane at a given temperature at $RH = 99\%$. The shape of the sorption curve is given by constant C .

5. Results

5.1. Convective Mass Transfer Coefficient

The mass transfer rate at the interface between a liquid or solid and a gas is often described as the convective mass transfer coefficient [18]. The convective resistance on both sides of the membrane plays an important role in the moisture transport performance but is usually neglected, resulting in less accurate data [7]. The convective mass transfer coefficient is related to the fluid dynamics of the cell.

As described previously, to obtain the moisture diffusivity in the membrane, the resistance in each step of the moisture transfer process needs to be evaluated. To obtain the resistance in the boundary layer between the membrane and the flowing air, measurements of the absent membrane were performed.

In Figure 5, it can be seen that the FLEC lower chamber is filled with distilled water. Conditioned air was supplied to the FLEC at volume flows ranging from 2 to 6 L/min. After the recorded relative humidity in the outlet became stable, the mean mass transfer coefficient was obtained. In this experiment, only the resistance caused by the flowing air was present; therefore, the total resistance was equal to the convective mass transfer resistance. The convective mass transfer coefficient k for each volume flow can be expressed as

$$R_T = R_c = \frac{1}{k} \quad (13)$$

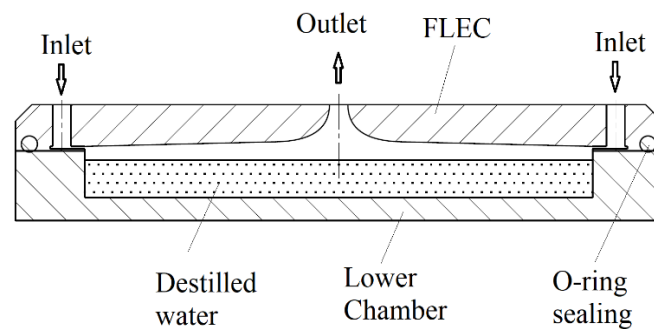


Figure 5. FLEC filled with distilled water.

In Figure 6, the convective mass transfer coefficient is plotted against the volume flow. The value of the Reynolds number for the volume flow of 2–6 L/min was in the range of 19 to 70. The increase in the volume flow through the cell caused a decrease in the relative humidity in the outlet. With the increased volume flow, the convective mass transfer increased.

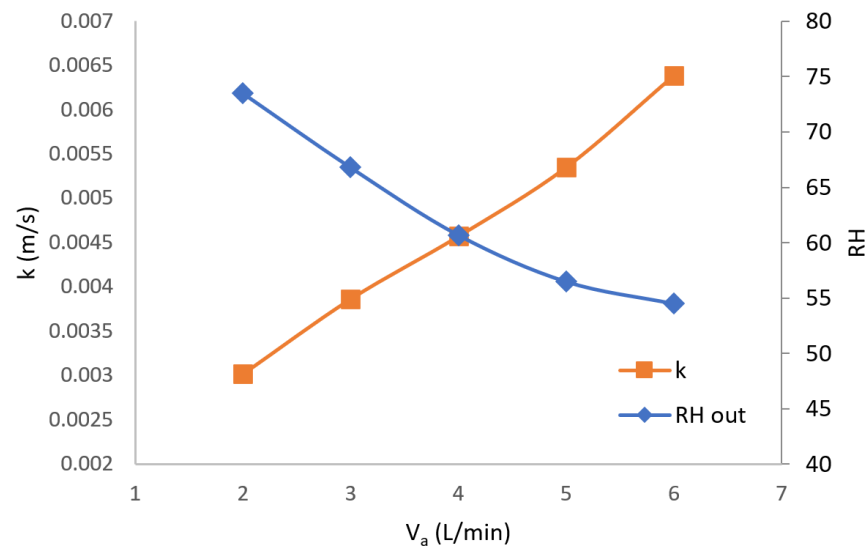


Figure 6. Convective mass transfer coefficient with varying airflow when no membrane used.

5.2. Resistance Caused by Air Gap

As shown in Figure 7, in this experiment, membrane samples were used. This time, the lower chamber was not filled with water and instead, a gap was created to prevent the membrane from being wetted by the water. The FLEC, membrane, and lower chamber created a sandwich-like structure to separate the water and flowing air. The volume flow for this experiment was set at a constant 4 L/min. By varying the air gap height from 4 to 11 mm, different total mass transfer resistances are obtained.

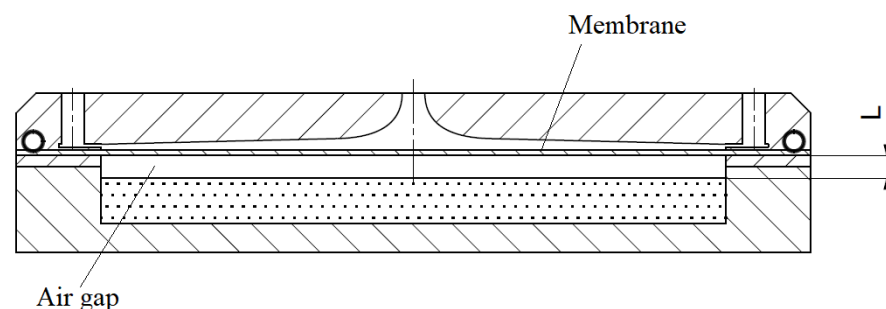


Figure 7. FLEC with membrane.

As shown in Figure 8, when the total mass transfer resistance is plotted against various air gap heights, a strong linear correlation between the total mass transfer resistance and the gap height can be seen. The equivalent diffusivity of the water vapor in the air can be obtained by calculating the slope of the regression line.

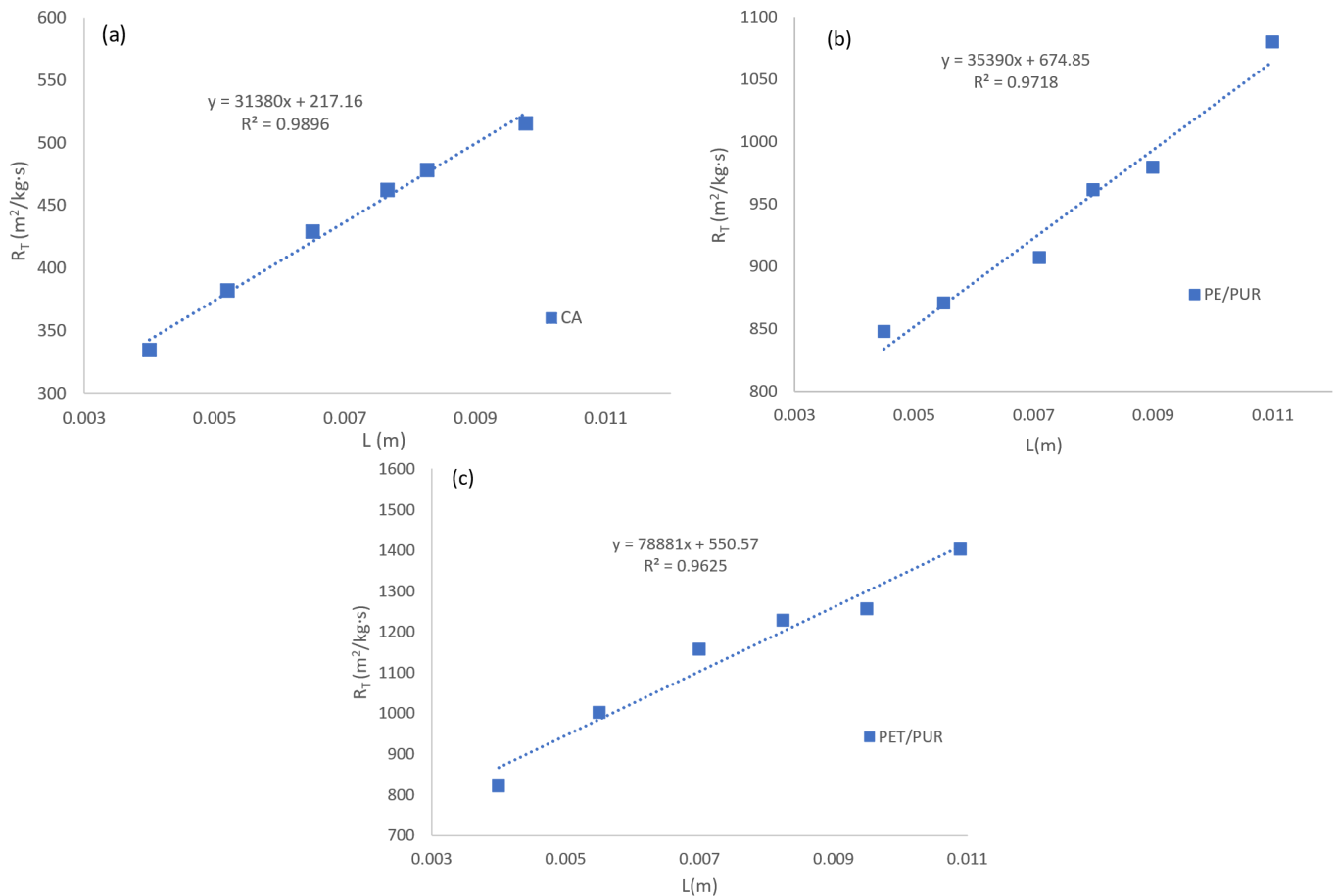


Figure 8. Total mass transfer resistances with various air gap heights (a) CA, (b) PE/PUR, (c) PET/PUR.

The calculated mean equivalent diffusivities of the water vapor in the air gap were $3.17 \times 10^{-5} \text{ m}^2/\text{s}$ for the cellulose acetate membrane, $3.3 \times 10^{-5} \text{ m}^2/\text{s}$ for the PE/PUR membrane, and $1.28 \times 10^{-5} \text{ m}^2/\text{s}$ for the PET/PUR membrane.

5.3. Moisture Diffusivity in the Membrane

A final experiment was performed to obtain the water vapor diffusivity in the membrane. The setup was similar to the previous experiment, except that the gap height was kept constant at 4 mm. The volume flow became a variable, as in the previous experiment, yielding volume flow from 2 to 6 L/min.

In Figure 9, the resistances of the moisture transfer in the membranes for the different airflows are presented. The membrane with the lowest total resistance was the CA membrane, which had half the resistance of the other two membranes. The reason for this was the small membrane thickness (20 μm) and high-water-adsorption potential of the membrane. The PET/PUR membrane showed a lower resistance than the PE/PUR, whereas the PE/PUR membrane showed on average a lower resistance to moisture transfer due to the different equivalent vapor diffusivity in the air gap. Such a deviation of the moisture diffusivity in the air gap was also observed by Min et al. [8]. It is important to mention, that the PE/PUR membrane was significantly thicker (150 μm) and showed only slightly higher resistance. The explanation is that the substrate's microporous structure

had high porosity (>60%). The small pore size of the substrate prevented coatings from being impregnated into the substrate, causing a thick, dense layer. The thick, dense layer acted as a gas barrier, decreasing the permeability of all gasses. Therefore, a very thin, dense layer on top of the substrate surface is preferable. On the other hand, the PET/PUR membrane's fibrous structure left little space for water vapor to pass in between the thick fibers, causing a smaller water vapor flux. Voids in between thick fibers allowed a coating to be impregnated into the substrate rather than stay on the surface, causing the thick, dense layer to prevent the water vapor from being diffused through the membrane. The way to increase the water vapor flux in the membrane is by using a substrate with finer fibers, having a higher porosity and lower thickness [15].

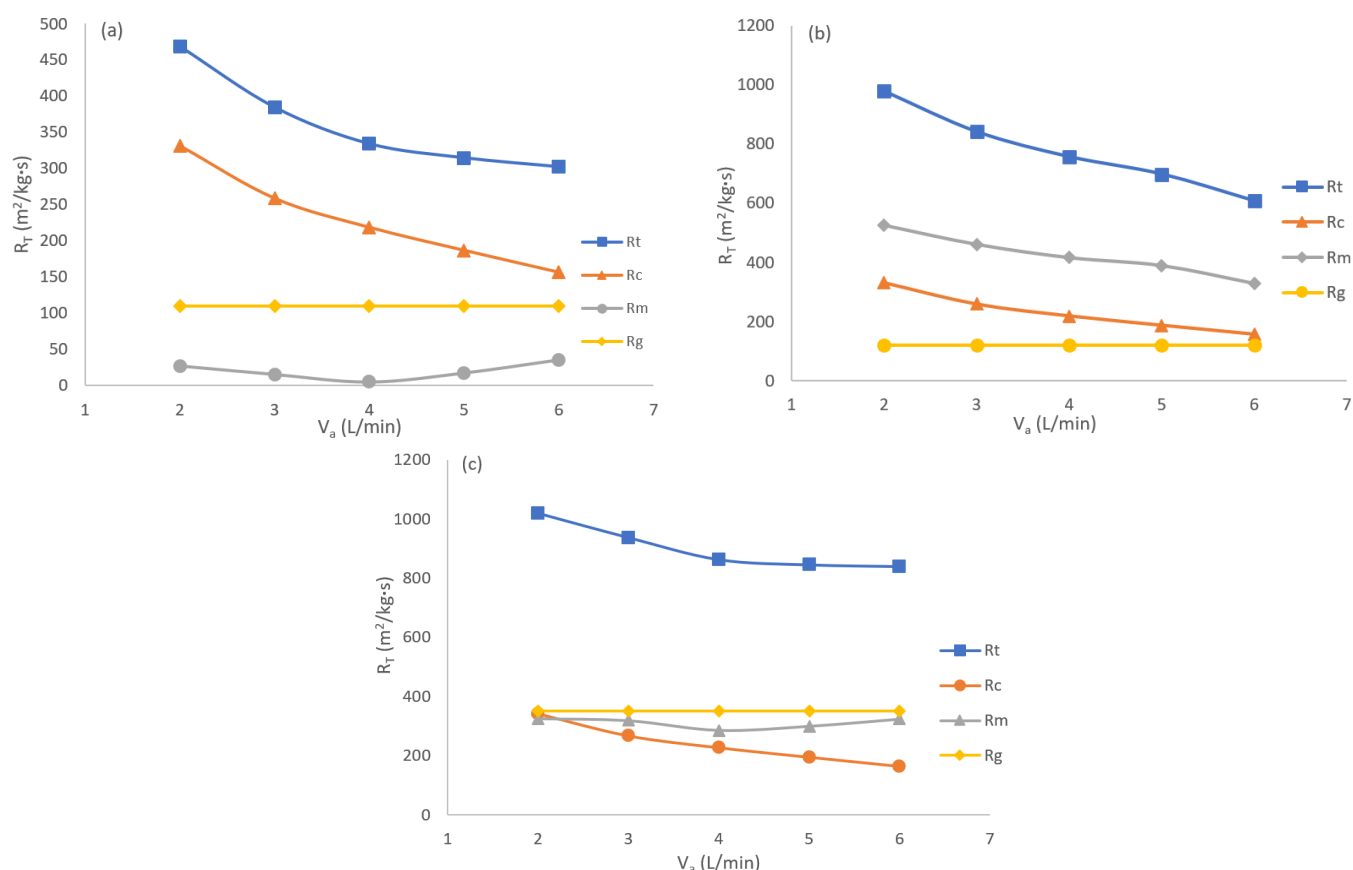


Figure 9. Mass transfer resistances for different airflows (a) CA, (b) PE/PUR, (c) PET/PUR.

According to Figure 10, the values of the water vapor diffusivity in the membranes were not constant and were dependent on the air humidity. By increasing the volume flow, the relative humidity in the outlet decreased and the mean air humidity simultaneously decreased. A similar correlation between the air humidity and membrane diffusivity was reported by Zhang [7], Gibson [19], and Koester [20]. The hydrophilic membranes aided with the adsorption and when exposed to high air relative humidity, the polymer chains inside the membrane tended to swell. The swollen polymer chains were pulled apart by the attached water molecules, creating so-called “water tunnels” through which water molecules could more easily penetrate through the membrane. This behavior was represented by the cellulose acetate membrane, which had a higher moisture uptake compared to the other two composite membranes. On the other hand, the diffusivity in the PE/PUR and PET/PUR membranes increased with the decrease in the outlet's relative humidity. This can be explained by the hydrophobic nature of the support layer, which causes water molecules to cluster on the polymer's surface instead of attaching to it. According to Koester [20], water clustering under higher relative humidity must have

a significant impact on water permeability since clustering preferentially occurs at high relative humidity.

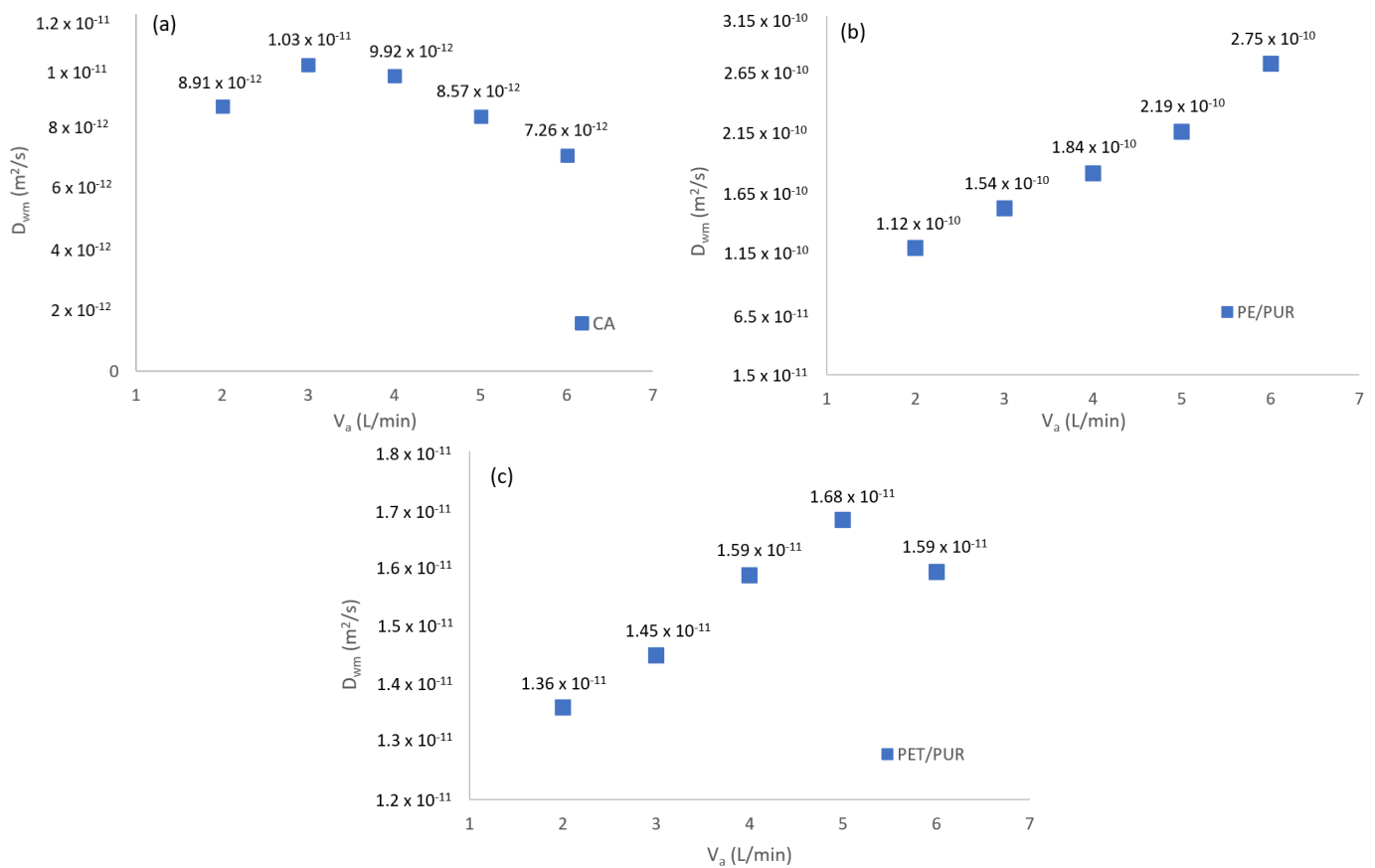


Figure 10. Diffusivities of various membranes: (a) CA, (b) PE/PUR, (c) PET/PUR.

The calculated mean values of the moisture diffusivities in the membranes were $6.55 \times 10^{-8} \text{ kg/m}\cdot\text{s}$ and $8.99 \times 10^{-12} \text{ m}^2/\text{s}$ for the CA membrane, $5.82 \times 10^{-8} \text{ kg/m}\cdot\text{s}$ and $1.9 \times 10^{-10} \text{ m}^2/\text{s}$ for the PE/PUR membrane, and $8.54 \times 10^{-9} \text{ kg/m}\cdot\text{s}$ and $1.53 \times 10^{-11} \text{ m}^2/\text{s}$ for the PET/PUR membrane. In Table 3, the values of the diffusivities are compared with the values published by other authors, which show agreement. By comparing the results from Table 3, it can be seen that the PE/PUR and CA membranes have high water vapor diffusivity values and the PET/PUR membrane has a moderate-to-low value.

Table 3. Comparison of water vapor diffusivities in the membranes.

Material	Membrane Thickness (μm)	Diffusivity ($\text{kg/m}\cdot\text{s}$)	Diffusivity (m^2/s)	Heat Conductivity ($\text{W/m}\cdot\text{K}$)	Reference
Paper	55	5.33×10^{-9}	-	0.44	[2]
Cellulose acetate CA	5	7.98×10^{-9}	-	0.41	[2]
Modified CA	5	2.5×10^{-9}	-	0.41	[2]
Composite PVDF/PVAL	107	-	3.2×10^{-11}	$0.197 + 0.152$	[10]
In this work					
Cellulose acetate CA	20	6.55×10^{-8}	8.99×10^{-12}	0.41	
PE/PUR	150	5.82×10^{-8}	1.9×10^{-10}	0.33	
PET/PUR	20	8.54×10^{-9}	1.53×10^{-11}	0.05	

6. Mathematical Model of the Exchanger

According to several studies, operating conditions and material properties have a significant influence on latent effectiveness. An analysis to determine the most influential parameters of heat and vapor transport was presented by Dugaria et al. [2]. The influence of the diffusivity, sorption coefficient, maximum water uptake, material heat conductivity, and membrane thickness were investigated. The increase in the moisture diffusivity in the membrane caused a significant increase in the latent heat flux. The sorption coefficient only had a minor effect on the mass transfer. The increase in the maximum water uptake increased the moisture transfer through the membrane. The fundamental solution for minimizing the moisture transfer resistance in the membrane is to reduce the membrane thickness. On the other hand, the membrane thickness and heat conductivity of materials show almost no influence on the sensible effectiveness.

Zhang et al. investigated the effect of the operating conditions on the latent and sensible effectiveness of a parallel-plates enthalpy exchanger [3]. Three membrane plates were investigated, showing similar values of sensible effectiveness. According to the results, it can be stated that operating conditions and material properties had little impact on sensible heat recovery. On the other hand, the moisture transfer was significantly influenced by the material properties, the most influential of which are the material thickness and sorption potential. The more hydrophilic a material, the higher the latent effectiveness that can be expected. Lee et al. [5] investigated the influence of airflow, humidity, temperature, and fin properties on heat and latent effectiveness. The values of the fin efficiencies for heat transfer were between 0.11 and 0.13. The fin efficiencies for the moisture transfer yielded much smaller values of between 0.006 and 0.014, whereas a higher efficiency was observed under heating conditions. The fin contribution to the mass transfer represented only 2%. The conduction resistance of the partition plate represented only 1% of the resistance due to the dominant convective resistance in the boundary layer. For the moisture transfer, however, the resistance in the membrane was dominant, with 72% and 76% under cooling conditions and 44% and 52% under heating conditions.

A mathematical model has been developed in this study to predict the heat and moisture transfer effectiveness and pressure drop of an air-to-air single pass membrane-based enthalpy exchanger with a cross-flow arrangement. The exchanger core was built into the separator/spacer configuration, as presented in Figure 11. The spacer was shaped in the form of a plain triangular fin surface. The spacer material was aluminum with a thickness of 0.135 mm, which provided mechanical stability to the exchanger core. The plate material properties were the same as the investigated membranes. The membrane properties were obtained from previous experiments and were used in the following calculations. Information about the core and surfaces is summarized in Table 4.

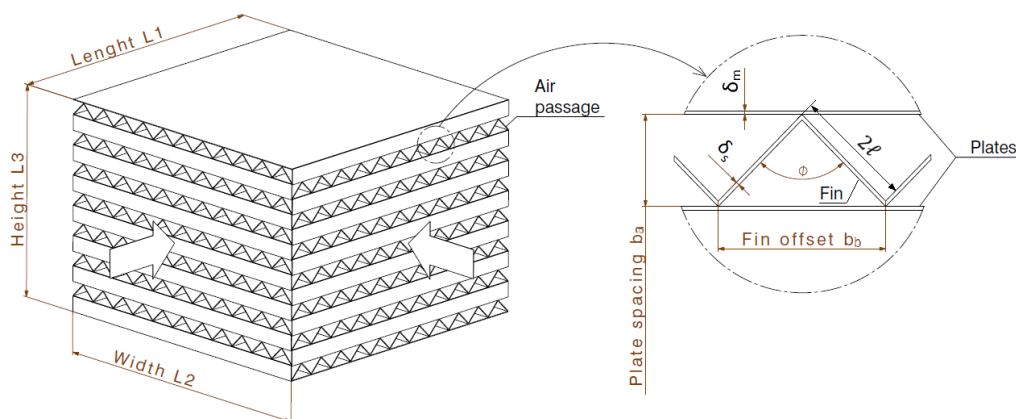


Figure 11. Cross-flow exchanger core.

Table 4. Exchanger core characteristics and operating conditions.

Total length L_1	500 mm	Inlet temperature H	35 °C
Total width L_2	500 mm	Inlet relative humidity H	46.60%
Total height L_3	500 mm	Inlet mass flow rate H	2000 m ³ /h
Fin thickness δ_s	0.135 mm	Inlet temperature C	23.89 °C
Membrane thickness δ_m	0.02 mm	Inlet relative humidity C	50.90%
Plate spacing b_a	2 mm	Inlet mass flow rate C	2000 m ³ /h
Fin offset b_b	1.22 mm	Inlet pressure H	95,500 Pa
Fin length $2l$	2 mm	Inlet pressure C	96,000 Pa
Number of passages N_p	247	Spacer/fin thermal conductivity λ_f	247 W/m·K
Total heat transfer area/volume between plates	3535 m ² /m ³		
Hydraulic diameter D_h	0.00137 m		
Free flow area/total front area \mathcal{G}	0.346		
Minimum free flow area A_o	0.1155 m ²		

6.1. Model Assumption

The mathematical model of the heat and mass transfer in the membrane-based enthalpy exchanger was based on the following assumptions:

- The heat and mass transfer processes are in a steady state.
- The heat conduction and water vapor diffusion along the flowing air direction are neglected.
- Moisture diffusion through the membrane is one-dimensional in direction (z).
- The physical properties of the membrane are constant.
- The water uptake of the membrane is in an equilibrium adsorption state

6.2. Heat Transfer Module

The mathematical derivation of the heat transfer was adopted from the effectiveness-NTU method. The correlations for the heat transfer module were adopted from the available literature [21]. The model was a rating problem with known geometry, flow arrangement, flow rates, and incoming fluid temperatures. The purpose of the model was to predict the thermal effectiveness and pressure drop of each air stream.

The density of the air is expressed as

$$\rho = \frac{p}{RT} \quad (14)$$

where the value of the gas constant of air R is 284.07 (J/kg·K); p is pressure in Pa; and T is the temperature in Kelvin (K).

The mass flow rate \dot{m} (kg/s) is defined as

$$\dot{m} = \dot{V}\rho \quad (15)$$

where \dot{V} is the volume flow of the air (m³/s) and ρ is the air density (kg/m³).

To obtain the properties of the air in the exchanger core, the sensible effectiveness of the exchanger must first be assumed. For the cross-flow arrangement, the usual sensible effectiveness $\varepsilon = 0.75$ can be expected [22].

The temperature of the leaving air with the assumed sensible effectiveness can be calculated as

$$T_{Ho} = T_{Hi} - \varepsilon(T_{Hi} - T_{Ci}) \quad (16)$$

$$T_{C,o} \approx T_{C,i} + \varepsilon \frac{\dot{m}_H}{\dot{m}_C} (T_{Hi} - T_{Ci}) \quad (17)$$

The average temperature of the cold and hot air can be calculated as

$$T_{H,m} = \frac{(T_{Hi} + T_{Ho})}{2} \quad (18)$$

$$T_{C,m} = \frac{(T_{Ci} + T_{Co})}{2} \quad (19)$$

The thermophysical properties of the hot and cold air are summarized in Table 5 and can be found in the thermophysical tables for air in [21].

Table 5. Thermophysical properties of the air.

	$\mu \times 10^3$ (Pa·s)	c_p (kJ/g·K)	Nu [23]	Pr	$Pr^{2/3}$
$T_{H,m}$ at 30.83 °C	187.7	1.007	2.2	0.713	0.798
$T_{C,m}$ at 27.89 °C	186.3	1.007	2.2	0.714	0.799
T_m at 29.88 °C	187.2	1.007	2.2	0.713	0.798

The Nusselt number for the triangular duct for the Prandtl number = 0.7 is calculated according to Equation (23).

The mass velocity G (kg/m²·s) is expressed as

$$G = \frac{\dot{m}}{A_o} \quad (20)$$

where A_o is the free flow area in (m²).

The definition of the Reynolds number is

$$Re = \frac{GD_h}{\mu} \quad (21)$$

The values of the Reynolds numbers for this calculation range from 66 to 230, representing the laminar flow in the channels of the exchanger core.

For the different fin types, the characteristic length L is different. For a plain, wavy, and offset fin, the characteristic length is defined by the hydraulic diameter D_h .

The definition of j is [24]

$$j = \frac{Nu}{RePr^{1/3}} \quad (22)$$

The Nusselt number can be obtained from the polynomial equation for a triangular (isosceles) duct for a fully developed laminar flow obtained from the literature [23].

$$Nu = 2.059 \left(\alpha^5 + 1.2489\alpha^5 - 1.0559\alpha^3 + 0.2515\alpha^2 + 0.1520\alpha - 0.0901 \right) / \alpha^5 \quad (23)$$

The relationship between the Reynolds number and friction factor for the isosceles triangular duct is

$$fRe = \frac{12(\alpha^3 + 0.2592\alpha^2 - 0.204\alpha + 0.0552)}{\alpha^3} \quad (24)$$

where α is the apex angle of the triangular duct (°).

The heat transfer rate at the interface between the solid and gas is described as the convective heat transfer coefficient h (W/m²·K⁻¹) and can be obtained from the calculated j factor:

$$h = \left(\frac{jGc_p}{Pr^{2/3}} \right) \quad (25)$$

where c_p is the specific heat (kJ/kg·K)

The coefficient m for the idealized plain triangular fin can be expressed as

$$m_h = \left(\frac{2h}{\lambda_f \delta_f} \right)^{1/2} \quad (26)$$

where λ_f is the heat conductivity of the fin material (W/m·K) and δ_f is the fin thickness (m).

The fin effectiveness for the heat transfer can be expressed as [5]

$$\eta_f = \frac{\tanh(mL_1)}{(mL_1)} \quad (27)$$

where L_1 is the fin length (m).

The overall surface efficiency is

$$\eta_o = \left[1 - (1 - \eta_f) \frac{A_f}{A} \right] \quad (28)$$

where A_f is the fin area and A is the total heat transfer area (m).

The separation plate conduction area A_m is expressed as

$$A_m = L_1 L_2 (2N_p + 2) \quad (29)$$

where N_p is the number of passages for the air.

The membrane heat resistance and overall conductance (K/W) can be expressed as

$$R_{h,m} = \frac{\delta_m}{\lambda_m A_p} \quad (30)$$

The $1/U_s A$ is

$$\frac{1}{U_s A} = \frac{1}{(\eta_o h A)_H} + R_m + \frac{1}{(\eta_o h A)_C} \quad (31)$$

To determine the NTU , first, C^* needs to be calculated:

$$C^* = \frac{C_{min}}{C_{max}} = \frac{(\dot{m} c_p)}{(\dot{m} c_p)} \quad (32)$$

The sensible NTU is

$$NTU_s = \frac{U_s A}{C_{min}} \quad (33)$$

where U_s is the total heat transfer coefficient (W/m²·K).

The following equation is proposed for the sensible effectiveness of the cross-flow exchanger [24]:

$$\varepsilon_{cross,S} = 1 - \exp \left[\frac{\exp(-C^* NTU_s^{0.78}) - 1}{C^* NTU_s^{-0.22}} \right] \quad (34)$$

6.3. Mass Transfer Module

Similar to the heat transfer module, the unmixed steady-state mass transfer form of ε - NTU equations is applied to the mass transfer module. The correlations for the mass transfer module were adopted mainly from the work of Zhang et al. [17] and Zhou et al. [24].

The latent effectiveness of the cross-flow arrangement can be written as

$$\varepsilon_{cross,L} = 1 - \exp \left[\frac{\exp(-R^* NTU_L^{0.78}) - 1}{R^* NTU_L^{-0.22}} \right] \quad (35)$$

In the case of the mass transfer, the specific heat ratio is replaced by the mass flow ratio R^* .

$$R^* = \frac{\dot{m}_{min}}{\dot{m}_{max}} \quad (36)$$

The number of transfer units (NTU) for the mass transfer is written as

$$NTU_L = \frac{U_L A}{R_{min}} \quad (37)$$

where U_L is the total mass transfer coefficient ($\text{kg}/\text{m}^2 \cdot \text{K}$) and A_m is the surface of the membrane (m).

The total moisture transfer resistance is described as individual resistances in series:

$$\frac{1}{U_L A} = \frac{1}{(\eta_o h_m A)_H} + \frac{\delta}{P_m A_m} + \frac{1}{(\eta_o h_m A)_C} \quad (38)$$

where k is the convective mass transfer coefficient ($\text{kg}/\text{m} \cdot \text{s}$), P_m is the membrane permeability ($\text{kg}/\text{m} \cdot \text{s}$), and η_o is the surface efficiency for the moisture transfer obtained by correlation:

$$\eta_o = \left[1 - (1 - \eta_f) \frac{A_f}{A} \right] \quad (39)$$

where A_f is the fin area.

The fin efficiency is expressed as

$$\eta_f = \frac{\tanh(mL_1)}{(mL_1)} \quad (40)$$

The coefficient m for the idealized plain triangular fin can be expressed as

$$m_h = \left(\frac{2h_m}{P_f \delta_m} \right)^{1/2} \quad (41)$$

where P_f is the fin permeability ($\text{kg}/\text{m} \cdot \text{s}$)

The moisture permeability of the fin is approaching zero due to the aluminum as the fin material. The fin efficiency for the moisture transfer is negligibly small even if the fin material is made from hydrophilic material [5].

The convective moisture transfer coefficient h_m ($\text{kg}/\text{m} \cdot \text{s}$) can be obtained using the Chilton–Colburn analogy with the convective heat transfer coefficient and Lewis number [5,25].

$$h_m = \frac{h}{Le^{2/3} \rho_a C_p} \quad (42)$$

The Lewis number is the ratio between the Schmidt and Prandtl numbers and its calculated value is around 1.15.

$$Le = \frac{Sc}{Pr} \quad (43)$$

The Schmidt number is defined as

$$Sc = \frac{\mu}{\rho D_{va}} \quad (44)$$

where μ is the dynamic viscosity of the air ($\text{kg}/\text{m} \cdot \text{s}$) and D_{va} is the water vapor diffusivity in the air (m^2/s). According to the literature, the value of the vapor diffusivity in the air at 25 °C is $2.6 \times 10^{-5} \text{ m}^2/\text{s}$.

The water uptake of the membrane at a given relative humidity is represented as:

$$\theta = \frac{\omega_{max}}{1 - C + \frac{C}{RH}} \quad (45)$$

The relative humidity and weight ratio of the moisture in the air are related with the following formula:

$$\omega = 0.622 \frac{RH p_s}{p_o - RH p_s} \quad (46)$$

where p_o is the atmospheric pressure (Pa) and p_s is the saturation vapor pressure (Pa).

The saturation vapor pressure at a given temperature can be expressed by the following correlation:

$$\ln p_s = \frac{C_1}{T} + C_2 + C_3 T + C_4 T^2 + C_5 T^3 + C_6 \ln T \quad (47)$$

The values of constants are $C_1 = -5800$, $C_2 = 1.3915$, $C_3 = 0.0486$, $C_4 = 0.4176 \times 10^{-4}$, $C_5 = -0.1445 \times 10^{-7}$, and $C_6 = 6.5460$ [8].

The membrane permeability (kg/m·s) is expressed as:

$$P_m = \frac{CD_{wm}\omega_{max}\rho_m e^{5294/T}}{10^6 \left(1 - C + \frac{C}{RH}\right)^2 RH^2} \quad (48)$$

From the calculated latent effectiveness, the relative humidity in the outlet of the hot air can be expressed as [22]:

$$\varepsilon_L = \frac{\dot{m}_H(\omega_{Hi} - \omega_{Ho})}{\dot{m}_{min}(\omega_{Hi} - \omega_{Ci})} \quad (49)$$

The total effectiveness from the mass flow and enthalpy of the wet air is [22]:

$$\varepsilon_T = \frac{\dot{m}_H(H_{Hi} - H_{Ho})}{\dot{m}_{min}(H_{Hi} - H_{Ci})} \quad (50)$$

where the enthalpy of the wet air is:

$$H = c_p T + \omega(2501 + 1.86T) \quad (51)$$

The pressure drop is calculated using the following formula:

$$\Delta p_H = \frac{G^2}{2g_c \rho} \left[\left(1 - \sigma^2 + K_c\right) + 2 \left(\frac{\rho_i}{\rho_o} - 1\right) + f \frac{L}{r_h} \rho_i \left(\frac{1}{\rho}\right)_m - \left(1 - \sigma^2 - K_c\right) \frac{\rho_i}{\rho_o} \right] p_i \quad (52)$$

where g_c is the proportionality constant in Newton's second law of motion, $g_c = 1$, and r_h is the hydraulic radius and can be expressed as $D_h/4$. The dimensionless contraction and expansion pressure loss coefficients for the flow at the heat exchanger entrance and exit K_c and K_e can be obtained from the frontal/free-flow area ratio \mathcal{G} , fin geometry, and Reynolds number [21].

7. Results

In this part of the study, the sensible and latent effectiveness of exchanger cores with different membranes were calculated. All the results were presented with the uniform temperatures and relative humidities in Table 4, simulating cooling under summer conditions. The diffusive properties of the three membranes were obtained experimentally in the previous section. The other thermophysical properties were summarized in Table 5.

7.1. Core with Different Membrane Materials and 20 μm Plate Thickness

In order to compare the influence of the membrane properties on the latent and sensible effectiveness, the uniform plate thickness was set at 20 μm . The volume flow was in the range of 500 to 3500 m^3/h and the pressure drop was in the range of 50 to 300 Pa. The plate spacing was fixed at 2 mm.

In Figure 12, the sensible effectiveness of the membranes and aluminum plate with a uniform thickness is compared. According to the results, there was a negligible effect of the heat conductivity of the plate material on the sensible effectiveness. The reason for this was the dominant convective resistance in the boundary layer compared to the heat conductivity of the material [3]. On the other hand, there was a significant effect of the membrane properties on the latent effectiveness, with the highest latent effectiveness found for the PE/PUR and CA membrane cores. The high latent effectiveness of the PE/PUR core was caused by the high water vapor diffusivity of the membrane. The CA core performance was more influenced by its higher sorption potential.

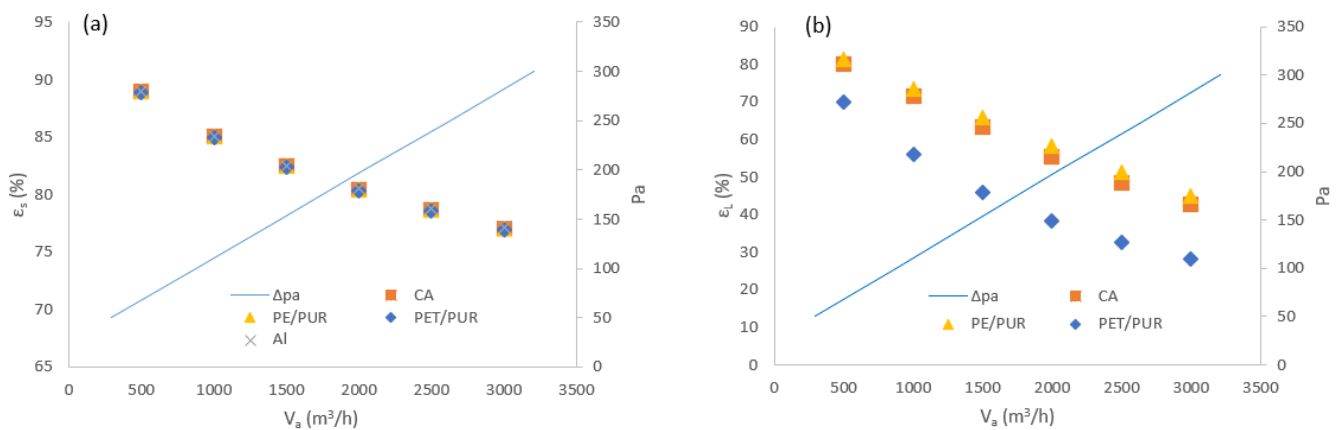


Figure 12. Effectiveness of exchanger cores under a variable airflow and a uniform membrane thickness of 20 μm . (a) Sensible effectiveness; (b) Latent effectiveness.

Effectiveness of the investigated membranes with thickness of 20 μm under given volume flow and pressure drop are summarized in Table 6. The sensible effectiveness of the PE/PUR core at a nominal volume flow of 2000 m^3/h and a 200 Pa pressure drop is 80.4% and 58.1% for the latent effectiveness.

Table 6. Summarized effectiveness of the cores with a 20 μm membrane thickness under nominal conditions.

	m^3/h	ΔPa	CA	PE/PUR	PET/PUR
ϵ_S	2000	200	80.5	80.4	80.3
ϵ_L	2000	200	55.5	58.1	38.3
ϵ_T	2000	200	65	66.6	54.3

7.2. Core with Different Membrane Materials and 100 μm Plate Thickness

Despite the latent effectiveness of the core with a 20 μm -thick plate being relatively high, the mechanical stability of such a core may not be sufficient to withstand the pressure difference between the airflows under standard operating conditions. A high-enough pressure difference can compress one of the air streams and in extreme cases, a blockage of one of the airstreams can occur. For this reason, considering the mechanical properties of the membrane, a thickness of 100 μm is preferable. In this section, the plate thickness was set to 100 μm with the operating conditions the same as in the previous section.

As seen in Figure 13, a strong correlation existed between the membrane thickness and latent effectiveness. Changing the membrane thickness from 20 μm to 100 μm caused

a decrease in the latent effectiveness by 18 to 67%, whereas the sensible effectiveness remained almost unchanged and the expected decrease ranged from 0.35 to 1.5%.

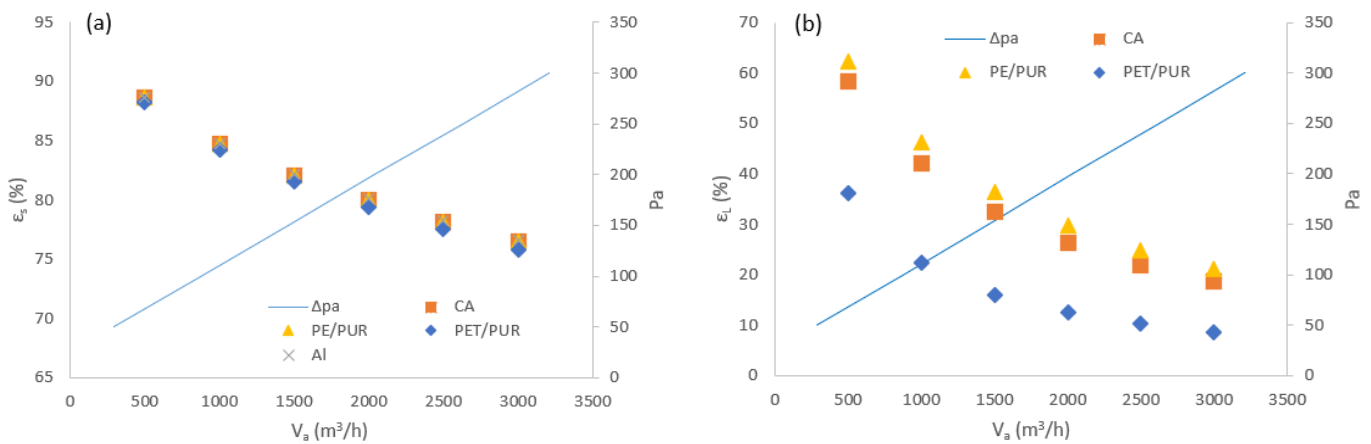


Figure 13. Effectiveness with a variable airflow and a uniform membrane thickness of 100 μm . (a) Sensible effectiveness; (b) Latent effectiveness.

Effectiveness of the investigated membranes with thickness of 100 μm under given volume flow and pressure drop are summarized in Table 7. The sensible effectiveness of the PE/PUR core at a nominal airflow of 2000 m³/h and a 200 Pa pressure drop was 80% and only 29.7% for the latent effectiveness.

Table 7. Summarized effectiveness of the cores with a 100 μm membrane thickness under nominal conditions.

	m ³ /h	ΔPa	CA	PE/PUR	PET/PUR
ϵ_S	2000	200	80	80	79.4
ϵ_L	2000	200	26.3	29.7	12.6
ϵ_T	2000	200	46.7	48.8	37.9

The increase in the membrane thickness significantly reduced the latent effectiveness. The sensible effectiveness remained almost unchanged. The total effectiveness decreased proportionally. As stated by Min et al. [25], an increased membrane thickness will cause increased thermal and moisture resistances. In order to reach the desired latent effectiveness at the current thickness, the membrane with the higher sorption potential and water vapor diffusivity should be used.

7.3. Influence of Different Plate Spacings

In this section, three different plate spacings were modeled to predict the core performance. The spacings of the 20 μm plates were 2 mm, 2.5 mm, and 3 mm. The pressure drop was unchanged by varying the fin offset and therefore the fin density for each plate spacing.

According to Figure 14, the increase in the plate spacing caused a drop in both the sensible and latent effectiveness, with the drop in the latent effectiveness being more significant. The drop in the effectiveness was caused mainly by the decrease in the transfer area of the core. The sharper drop in the latent effectiveness can be explained by the membrane's material having a greater contribution to the moisture transfer of the total moisture transfer than the heat conductivity of the total heat transfer in the core. Changing the plate spacing from 2 mm to 2.5 mm caused a decrease in the sensible effectiveness of 1.04% and up to 2.28% for various volume flows. The drop in the latent effectiveness of 2.6 and up to 18.83% was expected. Changing the plate spacing from 2 mm to 3 mm caused a decrease in the sensible effectiveness of 1.9% and up to 4.33%. and a drop in the latent effectiveness of 5.12% and up to 33.3%. For the PE/PUR core at a nominal airflow of

2000 m³/h and a pressure drop of 200 Pa, changing the plate spacing from 2 mm to 2.5 mm caused a drop in the sensible effectiveness of 1.72% and the latent effectiveness of 13.03%. Changing the plate spacing from 2 mm to 3 mm caused a drop in the sensible effectiveness of 3.23% and 24.33% for the latent effectiveness.

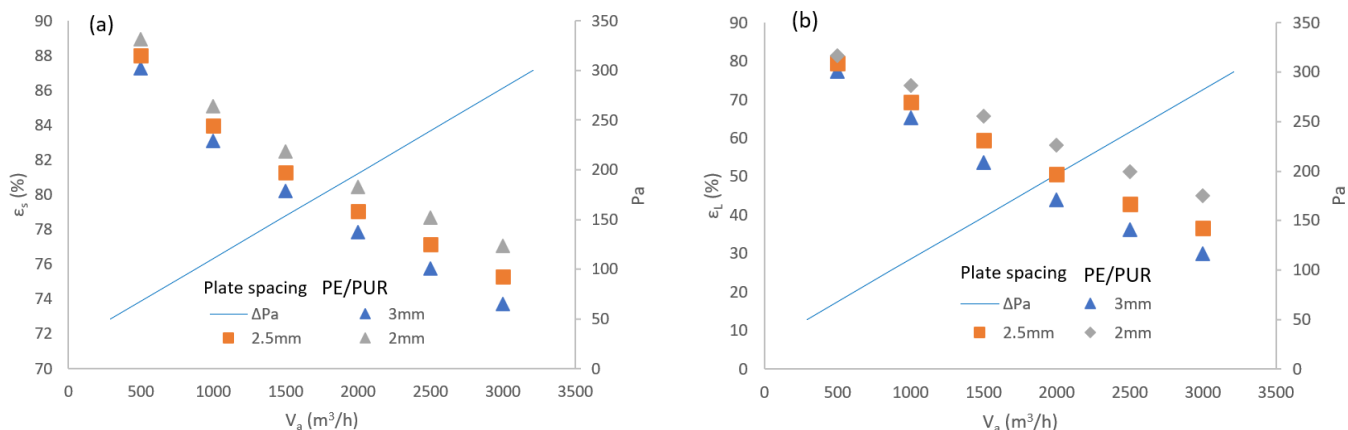


Figure 14. Effectiveness with variable plate spacing (a) Sensible effectiveness; (b) Latent effectiveness.

8. Conclusions and Discussion

In the first section, the values of the water vapor diffusivity of three polymer membranes with different structures and materials were experimentally obtained. The values of the water vapor diffusivity of the composite PE/PUR, PET/PUR, and CA membranes were compared, with the values presented by other authors showing agreement with the results in this study. The experiments showed that the PE/PUR and CA membranes had higher diffusivity than the PET/PUR membrane, which was mainly due to their preferable microstructure. However, the vapor diffusivity in the membrane was not the only factor influencing the water transport capability of the membrane. The second most influential parameter was the maximum water uptake of the membrane, followed by the constant representing the sorption curve. For practical applications, a high water sorption potential caused an increase in the membrane's weight and negatively influenced the mechanical properties. The high moisture content in the membrane promoted microbial growth. With the thicker PE/PUR membrane, the vapor transfer through the membrane material represented a major portion of the mass transfer resistance. With the thinner membrane, the convective resistance became more significant, although the very thin membrane lacked the strength necessary for proper operations and manufacturing processes.

The obtained and sampled data were used in the mathematical model of an enthalpy exchanger core to predict the latent and sensible effectiveness under various operating conditions and plate spacings. The results showed a minor influence of the heat conductivity and plate thickness on the sensible effectiveness if the plate was reasonably thin (100 μ m). The reason for this was the much higher contribution of the resistance in the boundary layer of the plate to the total heat transfer resistance. However, for the mass transfer, there was a significant influence of the membrane thickness and properties on the latent effectiveness. The thinner membrane created less resistance for moisture transfer. The higher the vapor diffusivity and maximum water uptake, the higher the flux of the moisture through the membrane; therefore, higher latent effectiveness of the membrane core can be expected. The increase in the plate spacing negatively influenced the sensible and latent effectiveness. With bigger spacing, less plates are required to build exchanger core, causing reduction of heat and the moisture transfer area. The fundamental approach to increasing the sensible and latent effectiveness is by increasing the transfer area, decreasing the membrane thickness, and decreasing the volume flow through the exchanger.

Author Contributions: K.K., investigation, data curation, conceptualization resources, writing—original draft; M.H., data curation, formal analysis, methodology, writing—review and editing, funding; and A.K., formal analysis. All authors have read and agreed to the published version of the manuscript.

Funding: This publication has been produced with the support of the projects KEGA 021ŽU-4/2021 Conversion of Primary Energy into Heat/Cold Using Thermodynamic Cycles and Compressor Circulation with the Working Substance (refrigerant) CO₂ and KEGA 032ŽU-4/2022—Implementation of Knowledge about Modern Ways of Reducing Environmental Burden in the Energy Use of Solid Fuels and Waste in the Pedagogical Process.

Institutional Review Board Statement: Not applicable.

Informed Consent Statement: Not applicable.

Data Availability Statement: Not applicable.

Conflicts of Interest: The funders had no role in the design of the study; in the collection, analyses, or interpretation of data; in the writing of the manuscript, or in the decision to publish the results. The authors declare no conflict of interest.

Nomenclature

List of characters		U_s	total heat transfer coefficient (W/m ² ·K)
A	area (m ²)	U_L	total mass transfer coefficient (m/s)
C	constant sorption curve	\dot{V}	volumetric flow (m ³ /s)
c_p	specific heat (kJ/kg·K)	Superscripts	
C_p	heat capacity (W/K)	*	dimensionless
C^*	heat capacity ratio	Greek letters	
D_{va}	diffusivity of water vapor in air (m ² /s)	δ	thickness (m)
D_{va}	equivalent diffusivity of water vapor in air (m ² /s)	θ	moisture content in membrane (kg/kg)
D_{vm}	moisture diffusivity in membrane (m ² /s)	λ	heat conductivity (W/m·K)
D_h	hydraulic diameter (m)	ψ	coefficient of diffusive resistance for membrane material
f	friction factor	μ	dynamic viscosity (Pa·s)
g_c	proportionality constant of motion	ω	humidity ratio (kg/kg)
G	mass velocity (kg/s)	η	efficiency
h	convective heat transfer coefficient kW	α	apex angle (°)
H	enthalpy (kJ/kg)	ϵ	effectiveness
J	water vapor permeation rate (kg/m·s)	$\Delta\omega$	logarithmic humidity ratio difference
j	factor of heat transfer	\mathcal{G}	free-flow area/frontal area
k	convective mass transfer coefficient (m/s)	Subscripts	
K_c	contraction pressure loss coefficient	a	air
K_e	expansion pressure loss coefficient	C	cold
L	length (m)	c	convective
Le	Lewis number	$cross$	cross-flow
\dot{m}	mass flow rate (kg/s)	f	fin
m	coefficient for fin geometry	H	hot
N_p	number of passages	i	In
Nu	Nusselt number	L	latent
p	pressure (Pa)	m	membrane, mean
P	permeability (kg/m·s)	o	out
Pr	Prandtl number	s	saturation
R	resistance (m ² ·s/kg)	S	sensible
R_h	heat resistance (K/W)	T	total
RH	relative humidity	w	water
r_h	hydraulic radius (m)	v	vapor
R^*	mass flow ratio	U_s	total heat transfer coefficient (W/m ² ·K)
Re	Reynolds number	U_L	total mass transfer coefficient (m/s)
Sc	Schmidt number	\dot{V}	volumetric flow (m ³ /s)
Sh	Sherwood number		
T	temperature (K)		

References

1. Review of Ecodesign and Energy Labelling—Ventilation Units. Available online: <https://www.nve.no/media/11694/2021-0222-em-cf.pdf> (accessed on 1 July 2022).
2. Dugaria, S.; Moro, L.; Del Col, D. Modelling heat and mass transfer in a membrane-based air-to-air enthalpy exchanger. *J. Phys. Conf. Ser.* **2015**, *655*, 12035. [[CrossRef](#)]
3. Zhang, L.Z.; Liang, C.H.; Pei, L.X. Heat and moisture transfer in application scale parallel-plates enthalpy exchangers with novel membrane materials. *J. Membr. Sci.* **2008**, *325*, 672–682. [[CrossRef](#)]
4. Lee, E.J.; Lee, J.P.; Kim, N.H. Moisture transfer characteristics of a LiCl-impregnated paper membrane used for an enthalpy exchanger. *J. Mech. Sci. Technol.* **2013**, *27*, 1527–1537. [[CrossRef](#)]
5. Lee, E.J.; Lee, J.P.; Sim, H.M. Modeling and verification of heat and moisture transfer in an enthalpy exchanger made of paper membrane. *Int. J. Air-Cond. Refrig.* **2012**, *20*, 1250015. [[CrossRef](#)]
6. Zhong, T.S.; Li, Z.X.; Zhang, L.Z. Investigation of Membrane-Based Total Heat Exchangers with Different Structures and Materials. *J. Membr. Sep. Technol.* **2014**, *3*, 1–10. [[CrossRef](#)]
7. Zhang, L.Z. Investigation of moisture transfer effectiveness through a hydrophilic polymer membrane with a field and laboratory emission cell. *Int. J. Heat Mass Transf.* **2006**, *49*, 1176–1184. [[CrossRef](#)]
8. Min, J.; Hu, T.; Liu, X. Evaluation of moisture diffusivities in various membranes. *J. Membr. Sci.* **2010**, *357*, 185–191. [[CrossRef](#)]
9. Zhang, L.Z. Heat and Mass Transfer in a Total Heat Exchanger: Cross-Corrugated Triangular Ducts with Composite Supported Liquid Membrane. *Numer. Heat Transf. Part A Appl.* **2008**, *53*, 1195–1210. [[CrossRef](#)]
10. Zhang, L.Z. Numerical study of heat and mass transfer in an enthalpy exchanger with a hydrophobic-hydrophilic composite membrane core. *Numer. Heat Transf. Part A Appl.* **2007**, *51*, 697–714. [[CrossRef](#)]
11. Zhang, L.Z. Evaluation of moisture diffusivity in hydrophilic polymer membranes: A new approach. *J. Membr. Sci.* **2006**, *269*, 75–83. [[CrossRef](#)]
12. Wolkoff, P. An emission cell for measurement of volatile organic compounds emitted from building materials for outdoor use—The Field and Laboratory Emission Cell (FLEC). *Gefahrst. Reinhalt. Luft* **1996**, *56*, 151–157.
13. Zhang, X.R.; Zhang, L.Z.; Liu, H.M.; Pei, L.X. One-step fabrication and analysis of an asymmetric cellulose acetate membrane for heat and moisture recovery. *J. Membr. Sci.* **2011**, *366*, 158–165. [[CrossRef](#)]
14. Huizing, R. Coated Membranes for Enthalpy Exchange and Other Applications. U.S. Patent 9.255,744 B2, 9 February 2016.
15. Huizing, R. Electrospun Nanofibrous Membranes for Water Vapour Transport Applications. Ph.D. Thesis, University of British Columbia, Vancouver, BC, Canada, 2017.
16. Wijmans, J.G.; Baker, R.W. The solution-diffusion model: A review. *J. Membr. Sci.* **1995**, *107*, 1–21. [[CrossRef](#)]
17. Zhang, L.Z. Progress on heat and moisture recovery with membranes: From fundamentals to engineering applications. *Energy Convers. Manag.* **2012**, *63*, 173–195. [[CrossRef](#)]
18. Steeman, H.-J.; T’Joel, C.; Van Belleghem, M.; Janssens, A.; De Paepe, M. Evaluation of the different definitions of the convective mass transfer coefficient for water evaporation into air. *Int. J. Heat Mass Transf.* **2009**, *52*, 3757–3766. [[CrossRef](#)]
19. Gibson, P. Effect of temperature on water vapor transport through polymer membrane laminates. *Polym. Test.* **2000**, *19*, 673–691. [[CrossRef](#)]
20. Koester, S. Membrane-Based Enthalpy Exchangers. Ph.D. Thesis, RWTH Aachen University, Aachen, Germany, 2017.
21. Shah, R.; Sekulic, S. *Fundamentals of Heat Exchanger Design*; John Wiley & Sons, Inc.: Hoboken, NJ, USA, 2003.
22. ASHRAE. *Air-to-Air Energy Recovery Equipment*; ASHRAE: Peachtree Corners, GA, USA, 2020; Chapter 26.
23. Hesselgreaves, J.E. *Compact Heat Exchangers, Selection, Design and Operation*; Butterworth-Heinemann: Oxford, UK, 2016; pp. 176–177.
24. Zhou, G.; Wang, J.; Zuo, W.; Fu, Y.; Zhou, X. Modeling air-to-air plate-fin heat exchanger without dehumidification. *Appl. Therm. Eng.* **2018**, *143*, 137–148. [[CrossRef](#)]
25. Min, J.; Su, M. Performance analysis of a membrane-based energy recovery ventilator: Effects of membrane spacing and thickness on the ventilator performance. *Appl. Therm. Eng.* **2010**, *30*, 991–997. [[CrossRef](#)]